



Stronger Southward Magnetic Field and Geoeffectiveness of ICMEs Containing Prominence Materials Measured from 1998 to 2011

Dongni Li and Shuo Yao¹ School of Geophysics and Information Technology, China University of Geosciences(Beijing), Beijing, 100083, People's Republic of China; yaoshuo@cugb.edu.cn*Received 2019 December 9; revised 2020 January 19; accepted 2020 January 20; published 2020 March 5*

Abstract

Interplanetary coronal mass ejections (ICMEs) could be classified into magnetic clouds (MCs) and non-MCs according to their magnetic field signatures, and into prominence-inside ICMEs (PIs) and non-PIs based on whether they contain colder and higher helium abundance plasmas than the solar wind. It is known that the MCs often lead to magnetic storms. However, whether or not the PIs have significant geoeffectiveness is unclear. This statistical work studies the southward interplanetary magnetic field (IMF) magnitude of the PIs, and the related magnetic storms' level. The data include the IMF and plasma moments measured by *ACE* and *WIND*, and the Dst index from 1998 to 2011. The hypothesis test based on the proportions of two groups is used to analyze 95 ICMEs related to single storms (SSs). The results show that the magnetic storms caused by the PIs mostly distribute at a strong level, while that caused by the non-PIs and by all the 95 ICMEs mostly distribute at a moderate level. The PIs have a significantly higher probability of generating SSs than the non-PIs. Moreover, the MCs containing carbon-cold and helium-enhanced materials (MC&PIs) have the highest fraction of minimum B_z , less than -11 nT. Since the MC&PIs have large-scale magnetic flux rope and prominence material, the stronger southward IMF is probably provided by the prominence. It is in accordance with the observed injection of enhanced twisted flux ropes to prominence. Therefore, the detailed eruption and propagation processes of the three-part coronal mass ejections deserve more concern from a space weather perspective.

Unified Astronomy Thesaurus concepts: [Solar coronal mass ejections \(310\)](#); [Solar prominences \(1519\)](#); [Space weather \(2037\)](#); [Geomagnetic fields \(646\)](#)

Supporting material: machine-readable table

1. Introduction

Coronal mass ejections (CMEs) are observable changes in coronal structure that occur within a few minutes to hours. They were first discovered in 1971 by the coronagraph on board the seventh *Orbiting Solar Observatory (OSO-7)*; Manchester et al. 2017). A CME can be identified by a new brightness enhancement (in white light) moving outward in a coronagraph image (Hundhausen et al. 1984; Yashiro et al. 2004). The typical geometry of CMEs is a three-part structure that contains a bright loop, a dark cavity, and a bright core. The three parts are usually interpreted as the plasma pile-up, the flux rope, and the eruptive prominence respectively (Illing & Hundhausen 1985; Hudson et al. 2006; Webb & Howard 2012). Several statistical studies reported that from 30% to 60% of the observed CMEs have three-part structures (Gopalswamy 2006; McCauley et al. 2015) And this three-part structure is the basic model in studying the initiation of the CMEs (Forbes 2000; Lin & Forbes 2000; Forbes et al. 2006; Manchester et al. 2017; Song et al. 2019).

When the CMEs propagate into the interplanetary space, their counterparts measured in situ are called interplanetary coronal mass ejections (ICMEs). ICMEs could be identified by stronger magnetic field, lower temperature of protons and electrons, enhanced helium abundances relative to protons,

bidirectional electrons, and occasional enhancement in minor ions of lower charge (Cane & Richardson 2003; Richardson & Cane 2004). However, these signatures do not necessarily occur simultaneously (Wimmer-Schweingruber et al. 2006; Zurbuchen & Richardson 2006; Richardson & Cane 2010). In previous studies, the ICMEs can be classified by the magnetic field structure. If the ICMEs have enhanced and smoothly rotating magnetic field during a long time, they are called magnetic clouds (MCs; Burlaga et al. 1981).

The materials inside a few ICMEs showing lower proton temperature, higher proton density, higher helium abundance, and lower charge state ions than the solar wind are considered to be the prominences (bright cores) of the CMEs (Hirshberg et al. 1972; Schwenn et al. 1980; Priest 1989; Lepri & Zurbuchen 2010; Yao et al. 2010; Song et al. 2016; Wang et al. 2018a). Feng et al. (2018) presented a new catalog based on the average charge state of carbon ions. If the ICMEs containing carbon ions with mean charge lower than the solar wind mean value minus three times standard deviation and the ionization temperature of carbon ions is lower than $10^{6.05}$ K, they are called carbon-cold ICMEs (CCs). The CCs take about one-third of the studied ICMEs. Therefore, the ICMEs could also be classified by ion composition.

The CMEs propagating along the earthward direction are halo CMEs. Interplanetary counterparts of the halo CMEs are the most important phenomena that drive geomagnetic storms (Gopalswamy et al. 2007; Kilpua et al. 2017b). Geomagnetic storms feature a strong disturbance on the horizontal component of global geomagnetic field lasting for tens of hours to days. The Dst index represents the horizontal magnetic field variation caused by an enhanced ring current

¹ Corresponding author.

during the storm (Sugiura 1964). And its minimum value is used to estimate the storm intensity. A geomagnetic storm could be typically divided into three phases including the sharp increase of the Dst index as the initial phase, the decrease of the Dst as the main phase, and then the recovery phase (Gonzalez et al. 1989, 1994; Yokoyama & Kamide 1997; Maltsev 2004; Gopalswamy 2006; Nikolaeva et al. 2012; Monreal MacMahon & Llop-Romero 2014). Statistical studies reported that the Dst minimum is related to the magnitude of the southward ($B_z < 0$) interplanetary magnetic field (IMF; Burton et al. 1975; Akasofu 1981; Yermolaev et al. 2010; Adekoya & Chukwuma 2018).

Since the MCs have a large-scale magnetic flux rope, many researchers studied the geoeffectiveness of the MCs and the non-MCs. Statistical results showed that the MCs are the most geoeffective subset compared to the non-MCs, corotational interaction region (CIR), fast solar wind, and shock (Kilpua et al. 2017a, 2017b). Furthermore, the intensity of the geomagnetic storm caused by the MCs is also stronger than that of the other types mentioned above (Echer et al. 2005; Zhang et al. 2007; Nikolaeva et al. 2011).

However, the geoeffectiveness of the PIs and the non-PIs has not been studied so far. To examine if the PIs are a real physical subset of ICMEs or an artificial one by ion composition criterion, it is necessary to check their effect on the geomagnetic field and their forming mechanism on the solar atmosphere. Since the PIs represent the CMEs with the prominence eruption, it is also interesting to investigate if the details of the eruption process of the three-part CMEs deserves more attention from the space weather perspective.

In this work, we perform a statistical analysis on the southward IMF of the 95 single ICMEs and on the intensity of the storms caused by them measured from 1998 to 2011. The data and the criteria used to identify the storms are described in Section 2. The statistical results of the storm intensity and IMF B_z are shown in Section 3. The possible mechanisms are discussed in Section 4. Finally, the conclusion is given in Section 5.

2. Data and Method

2.1. Data

In this work, we use the IMF measurements, solar wind proton (N_p), α particle density (N_α), and the geomagnetic indices. The B_z component of the ICMEs in the Geocentric Solar Ecliptic (GSE) coordinate system, and the number density of solar wind protons and α particles are available on CDAWEB (<https://cdaweb.gsfc.nasa.gov/index.html>). The IMF B_z component is level 2 (verified) data measured by the magnetic field experiment (MAG; Smith et al. 1998) on board the ACE spacecraft having a temporal cadence of 1 hr. The N_α/N_p is measured by the solar wind electron proton alpha monitor (SWEPA; McComas et al. 1998) on board the ACE spacecraft, having a temporal cadence of 64 s. Since there are data gaps caused by measurement failure on ACE data, and the WIND spacecraft is very close to ACE, the WIND data is also used. The 92 s-cadence N_α (n/cc) and N_p (n/cc) from nonlinear analysis are measured by the solar wind experiment (SWE; Ogilvie et al. 1995) on board the WIND spacecraft. The Dst index is derived from hourly averaged horizontal magnetic field variation at low latitude (Sugiura 1964). It is provided by

WDCG (World Data Center for Geomagnetism) in Kyoto (<http://wdc.kugi.kyoto-u.ac.jp/dst/dir/index.html>).

2.2. ICME List and Event Selection

First, the studied ICMEs are from the 219 ICMEs in Feng et al. (2018) including 69 CCs and 99 MCs measured from 1998 February to 2011 August. Second, we check the geomagnetic variation caused by these ICMEs according to their Dst index. Considering the traveling time of the ICMEs from ACE/WIND spacecraft to the Earth, there is about a 2 hr delay in the Dst response (Zhang et al. 2007; Yermolaev et al. 2010).

Based on previous studies, we quantify the criteria of different types of geomagnetic disturbances caused by the ICMEs. Since not all the storms have the initial phase, we focus on the main phase and the recovery phase. The start of the main phase is fixed by the maximum Dst value between the ICME shock and the minimum Dst. The minimum Dst called Dst_{\min} marks the end of the main phase and the start of the recovery phase. We define the end of the recovery phase as the Dst approaching 10% of the Dst_{\min} for $Dst_{\min} > -60$ nT or approaching 30% of the Dst_{\min} for $Dst_{\min} \leq -60$ nT. At the end of the recovery phase, we require that $Dst > -30$ nT. This means that the negative Dst must have an absolute value less than 30 nT, otherwise the Dst should be positive (Yokoyama & Kamide 1997). To guarantee the unique correspondence between the ICMEs and the magnetic storms, we divide the geomagnetic variations caused by ICMEs into four types: single storms (SSs), multiple storms (MSs), storm-like disturbances (SDs), and non-storms (NSs), shown in Figure 1.

The geomagnetic disturbances showing $Dst_{\min} > -30$ nT are identified as NSs. The geomagnetic disturbances having the main phase and recovery phase, when there is only one ICME, are classified as SSs. It should be noted that there are some additional constraints to select SSs: (1) The onset of the main phase should be at a relatively quiet level ($Dst > -30$ nT). Meanwhile, the Dst decrease amplitude in the main phase should be greater than 30 nT. (2) The Dst_{\min} should occur between the shock time and 3 hr after the end time of ICMEs. (3) There must be no other ICMEs during the recovery phase.

The long-lived MSs are caused by two or more continuous ICMEs. They have the main phase and the recovery phase with $Dst_{\min} \leq -30$ nT (Xie et al. 2006). The geomagnetic disturbances that do not meet any of the above criteria for SSs, MSs, and NSs are classified as SDs. As a result, 95 single storms are identified. The 95 single ICMEs out of the 219 ICMEs are related to the SSs. They are selected to carry on the statistical analysis, shown in Figure 2. In this study, we analyze the levels of single storms caused by different types of ICMEs. We use the Dst_{\min} to classify the intensity of storms into five levels based on Loewe & Pröls (1997): weak (-50 nT $< Dst_{\min} \leq -30$ nT), moderate (-100 nT $< Dst_{\min} \leq -50$ nT), strong (-200 nT $< Dst_{\min} \leq -100$ nT), severe (-350 nT $< Dst_{\min} \leq -200$ nT), and great ($Dst_{\min} \leq -350$).

Additionally, we divide all the 219 ICMEs into different types according to their magnetic field structure, carbon ionic charge state, and the helium abundance relative to protons. We adopt the criteria from Burlaga et al. (1981) and Feng et al. (2018) to identify MCs. Considering the prominence is colder and the presence of helium enhanced chromospheric material, we focus on the two signatures that could be identified as prominence-inside ICMEs (PIs): the carbon cold and the

Four Types of Geomagnetic Field Response Caused by ICMEs

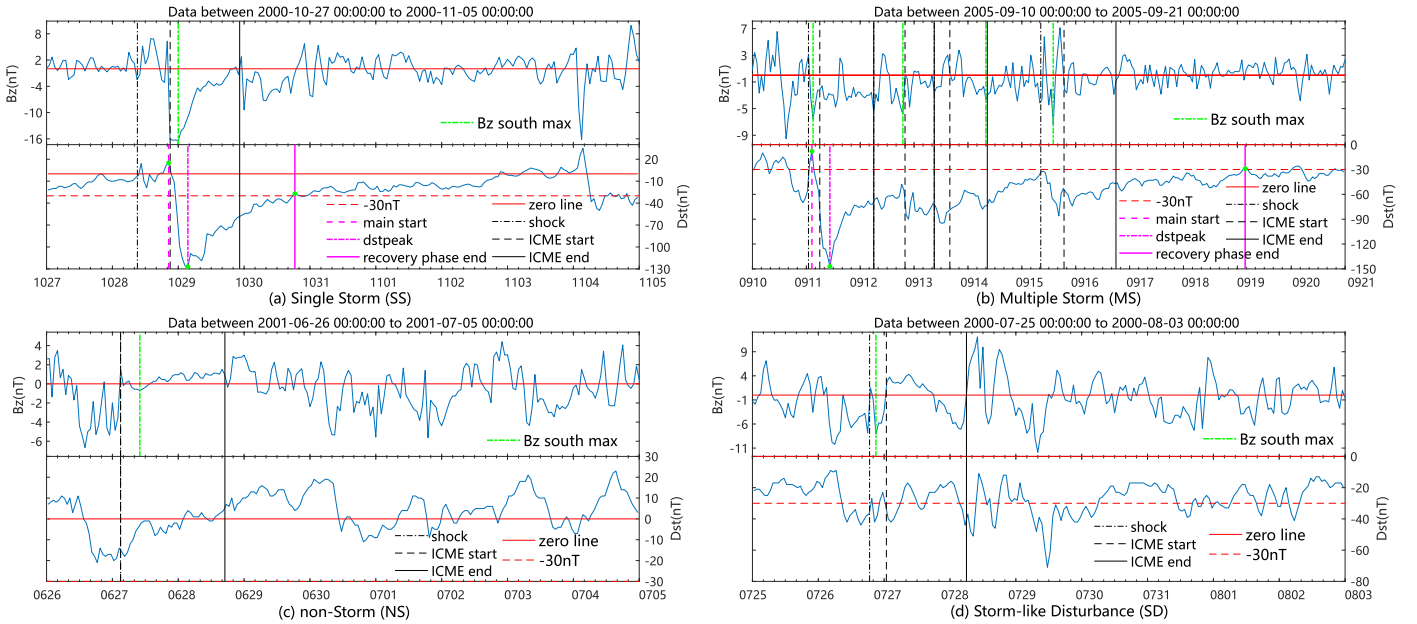


Figure 1. Four types of geomagnetic disturbances caused by 219 ICMEs. Subfigures show the typical Dst time variation of (a) the single storms; (b) the multiple storms; (c) the non-storms; and (d) the storm-like disturbances. The ICMEs are between the first black dotted–dashed line and the last black solid line. The duration of the single storm in Figure 1(a) and the multiple storm in Figure 1(b) is between the pink dashed line and the pink solid line.

helium enhanced plasmas. The ICMEs containing carbon cold materials (CCs) are obtained from the list in Feng et al. (2018). According to Zurbuchen et al. (2016) and Wimmer-Schweingruber et al. (2006), the plasmas with $N_\alpha/N_p > 0.08$ are possible prominence materials. Therefore, we use this criterion to identify the helium enhanced (HEs) ICMEs. In addition, since the measured N_α has large uncertainty, we require the $N_\alpha/N_p > 0.08$ lasting for 2 hr inside the ICMEs. In all the 219 studied ICMEs from 1998 to 2011, there are 99 MCs, 69 CCs, and 69 HEs shown in Figure 2. In the 95 ICMEs causing single storms, there are 55 MCs, 39 CCs, and 37 HEs. 17/95 ICMEs are simultaneously CCs and HEs, and 12/95 ICMEs are simultaneously MCs, CCs, and HEs, listed in Table 1. In addition, the detailed information of the 95 ICMEs and the related single storms are provided in Table 2 in the Appendix.

2.3. Method

We use three statistical methods to quantify the significant differences between different types of ICMEs. The original information that we obtain is the proportion of ICMEs causing SSs to the total number of certain types of ICMEs. However, different proportions could be generated by a random process. Moreover, different proportions do not necessarily mean different probabilities. To reveal the statistical significance of the different proportions from different types of ICMEs, we first calculate the probability of the random process. In statistics, it is assumed that the event with small probability does not occur. If the probability is smaller than 0.05, it could be interpreted that a certain proportion is not controlled by random process at a 95% confidence level. Second, we use one of the hypothesis tests on two groups to check if the higher proportion represents the higher probability. It is the Z-test (the chi-squared test) based on proportions of the independent two groups assuming the probabilities are the same (Shewart &

Wilks 2004).

$$Z = \frac{(p_1 - p_2) - (q_1 - q_2)}{\sqrt{\frac{q_1(1-q_1)}{n_1} + \frac{q_2(1-q_2)}{n_2}}}. \quad (1)$$

In the equation, p_1 and p_2 are the proportions for group 1 and group 2 having certain signatures. The probabilities of the independent two groups are represented by q_1 and q_2 , which are assumed to be the same as $q_1 = q_2$. The sample numbers are n_1 and n_2 for the two groups. At the 95% confidence level, if the Z value is larger than 1.645, the null hypothesis could be denied. This means that the different ratios of events with certain signatures to the total number in the two groups have statistical significance. The group having a larger proportion has larger probability. The other original result is the distribution of single storms caused by different subtypes of ICMEs on the Dst_{\min} and IMF B_z . To examine how significant the difference between the two groups is, we adopt the Kolmogorov–Smirnov test (KS-test) (Massey 1951; Miller 1956; Marsaglia et al. 2003). The key parameter of the test is the p -value between the cumulative fraction function of the two distributions. If the p -value is smaller than 0.05, the two distributions are statistically different at the 95% confidence level.

3. Result

In the studied 219 ICMEs, 95 ICMEs caused the SSs and 56 ICMEs caused the NSs, listed in Table 1. These 151 ICMEs could be divided into the CCs and the non-CCs, and HEs and non-HEs according to their carbon ionic charge and the helium abundance. Also, they could be divided into the MCs and the non-MCs according to their magnetic field structure. The numbers of ICMEs in each catalog are shown in Figure 2. In the ICMEs causing the 95 single storms, there are 55 MCs and 40 non-MCs, 39 CCs and 56 non-CCs, or 37 HEs and 58

The Type of Geomagnetic Response Caused by ICME (Samples Size:219 ICMEs)

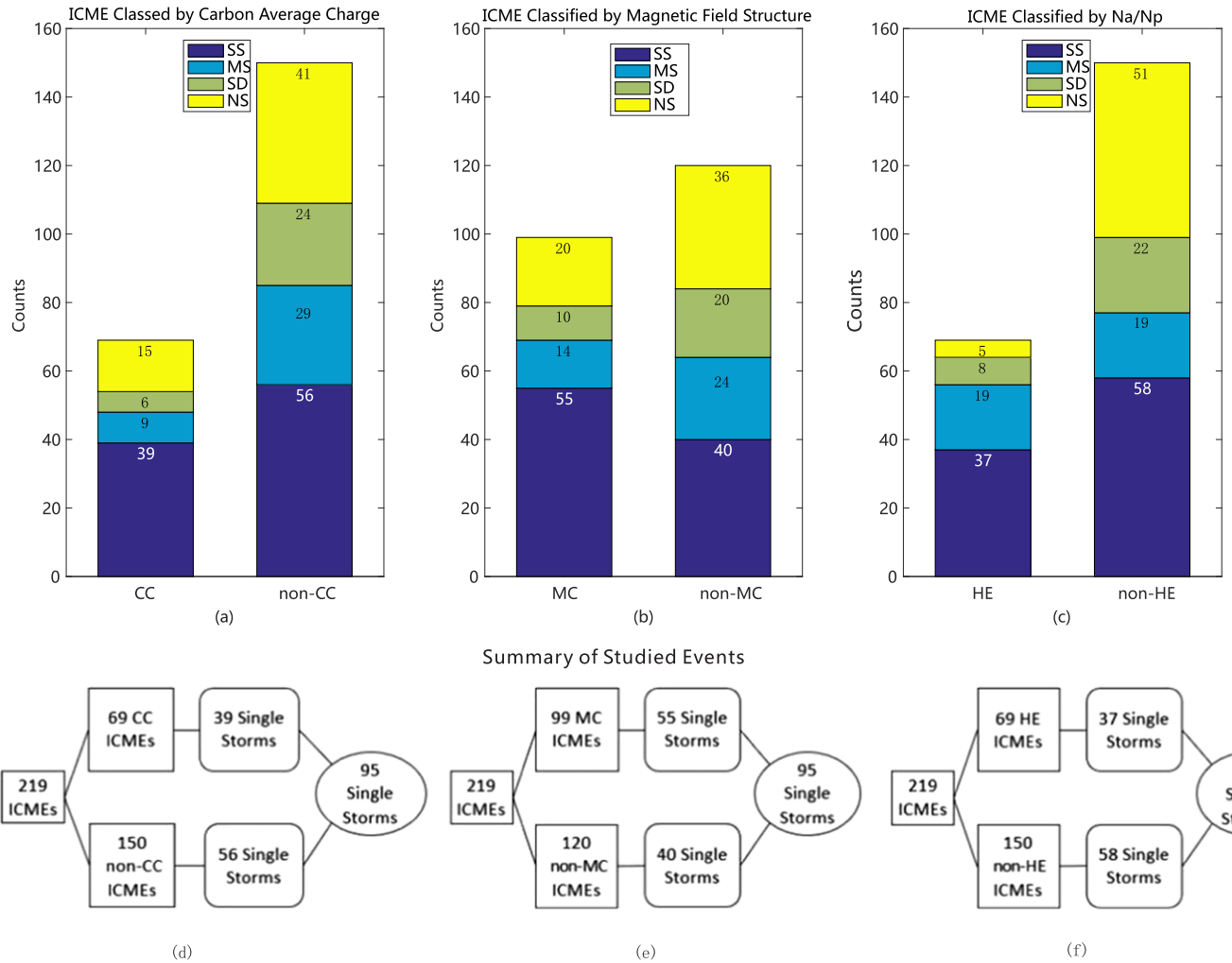


Figure 2. Number of different types of ICMEs measured from 1998 to 2011. Panels (a)–(c) are the distributions on the four types of geomagnetic field disturbances caused by CCs and non-CCs, MCs and non-MCs, and HEs and non-HEs, respectively. Panels (d)–(f) are the studied 95 single ICMEs out of 219 ICMEs in three catalogs based on carbon ionic charge, magnetic field structure, and N_{α}/N_p .

Table 1
The Counts and Fraction of Different Types of ICMEs

Types of ICMEs	All	SSs(fraction)	NSs(fraction)	MSs	SDs
ALL	219	95(0.43)	56(0.26)	38	30
CC&MCs	38	26(0.68)	6(0.16)	4	2
non-CC&MCs	61	29(0.47)	14(0.23)	10	8
CC&non-MCs	31	13(0.42)	9(0.29)	5	4
non-CC&non-MCs	89	27(0.30)	27(0.30)	19	16
CC&MC&HEs	15	12(0.80)	2(0.13)	1	0
non-CC&non-MC&non-HEs	66	18(0.27)	25(0.38)	12	11
CC&HEs	28	17(0.61)	3(0.11)	6	2

non-HEs. In the 56 ICMEs causing non-storm, there are 20 MCs and 36 non-MCs, 15 CCs and 41 non-CCs, or 5 HEs and 51 non-HEs.

We make the Z-test on the proportions of the CCs (39/69) and non-CCs (56/150), and that of HEs (37/69) and non-HEs (58/150), causing single storms, assuming the probabilities of the two groups are the same. The Z values are 2.76 and 2.07, which are larger than the critical value at the 95% confidence level: $Z_{0.05} = 1.645$. This means that the null hypothesis

should be rejected. Thus, the probability of the CCs or the HEs to generate single storms is significantly higher than the non-CCs or the non-HEs. Next, we use the same hypothesis test on the proportions of the MCs (55/99) and the non-MCs (40/120) groups. The Z value is 3.43, which is also larger than 1.645. It is in accordance with the previous studies that the MCs have higher probability of causing geomagnetic storms than the non-MCs. Finally, we make the Z-test on the proportions of NSs occurrence in different types of ICMEs. Obviously, fewer CCs, MCs, and HEs generate non-storms than their opposite types. However, except for the HEs, the other two types do not show statistical significance at the 95% confidence level.

Furthermore, we analyze the intensity of 95 SSs caused by various types of ICMEs. The intensity of SSs is described by Dst_{min} . We classify the SSs into five levels according to their Dst_{min} : weak, moderate, strong, severe, and great. The counts and fraction of each level of single storms caused by the MCs and CCs are shown in Figure 3. Figure 3(a) shows the distribution of all 95 SSs in five levels. It is obvious that the fraction of moderate SSs is the largest in the 95 SSs. In Figures 3(c) and (g), the distributions of non-CCs and

Distribution of Single Storm Type on Storm Level (Samples Size:95 Single Storms)

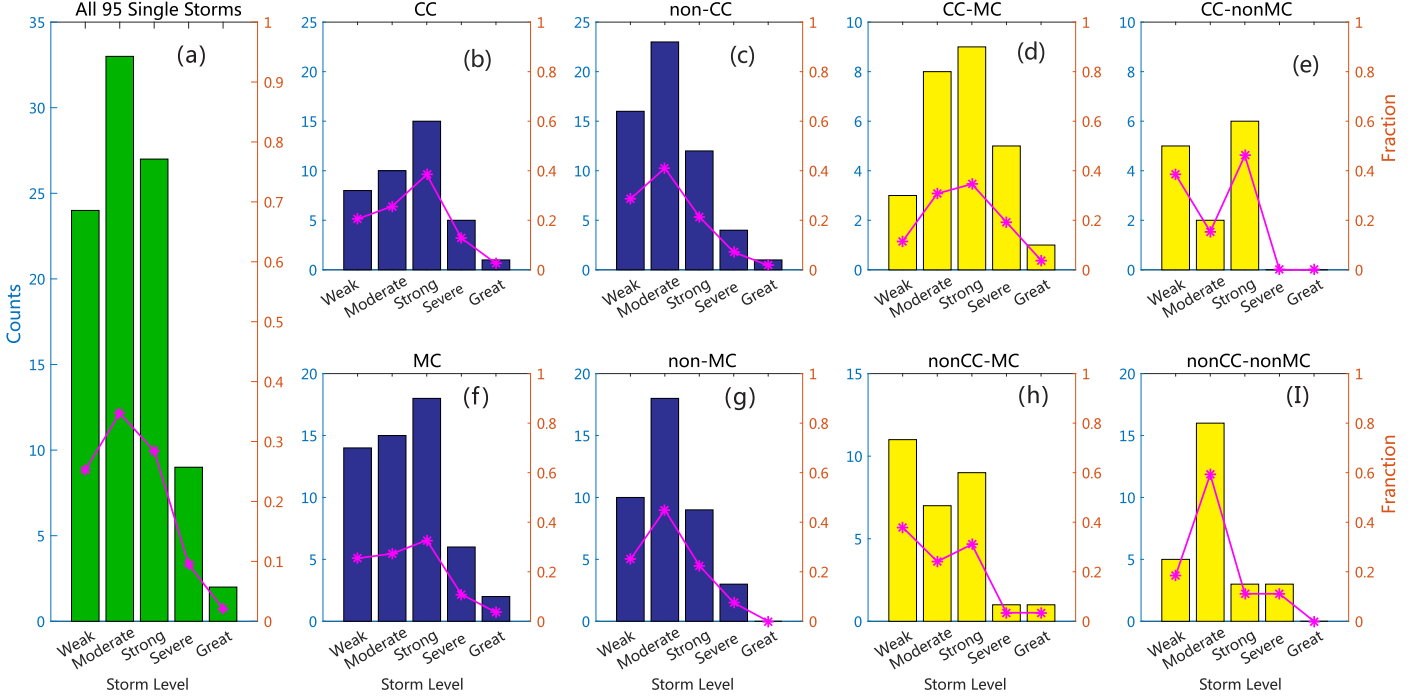


Figure 3. Distribution of 95 SSs caused by different types of ICMEs on storm levels. All panels have double y-axes; the left one denotes the counts of the SSs at each level and the right one denotes the fraction. The histograms show the counts. The pink lines show the fractions.

non-MCs have a similar trend with 95 SSs in that they concentrate on the moderate level. However, Figures 3(b) and (f) show the different distribution trends from that of 95 SSs. The CCs and MCs are most likely to cause strong SSs compared to the non-CCs and the non-MCs, respectively. It should be mentioned that there are 26/95 ICMEs that are simultaneously CCs and MCs (CC&MCs). The single storms caused by ICMEs classified as HEs are also investigated, as shown in Figure 4. It is obvious that the HE, CC&HE, and MC&HE tend to generate strong storms. More interesting, the CC&MC&HE is most likely to generate a severe storm.

To compare the difference of the SSs caused by MCs, CCs, HEs, and CC&MC&HEs, we obtain the cumulative distribution of Dst_{\min} of 95 SSs. The result is shown in Figure 5. It is obvious that the CC&MC&HEs have the highest cumulative fraction. The HEs have the second highest fraction followed by the CCs and MCs. The non-MCs, non-CCs, and non-HEs have the least fraction in similar trend. Both the storm level distribution and the Dst_{\min} cumulative distribution indicate that the single storms caused by the CC&MC&HEs are obviously stronger than the others.

As far as we know, the MCs are ICMEs with a magnetic flux rope. Thus they tend to have strong negative B_z causing magnetic storms. However, the classification of CCs and HEs is not based on the magnetic field structure but on the presence of prominence material. Why the CC&MC&HEs have the strongest geoeffectiveness is a question that deserves further investigation. To reveal the differences of the CCs, HEs, and MCs, we further classify the 95 ICMEs causing SSs into combination subsets, listed in Table 1.

We notice that CC&MC&HEs have the largest proportion (0.80) to cause the SSs, and they have the second smallest

proportion (0.13) to cause the NSs. If we assume the different proportions are generated by random processes, we find that the two probabilities of CC&MC&HEs causing SSs and NSs are $\frac{C_{95}^2 C_{124}^4}{C_{219}^{15}} \approx 0.0028$ and $\frac{C_{26}^2 C_{163}^{13}}{C_{219}^{15}} \approx 0.1449$. Such a small probability means that the CC&MC&HEs tending to cause SSs is not controlled by a random process at the 95% confidence level. It is not a random process for the CC&MC&HEs to generate non-storms at the 85% confidence level. Next, we use the Z-test to check if the differences between the proportions of the SSs and NSs caused by CC&MC&HEs and non-CC&non-MC&non-HEs are statistically significant. The Z values are 3.72 and 1.97, respectively, which mean that the CC&MC&HEs do have a higher probability of causing SSs, and have a smaller probability of causing weak magnetic disturbance, at 95% and 85% confidence levels, respectively. Above all, we suppose that the CC&MC&HEs are the most geoeffective of the studied ICMEs.

4. Discussion

The statistical analysis results show that both the CCs and MCs tend to generate stronger storms, and together they have a larger probability to generate storms than each alone. Since the reason for the MCs to generate a strong magnetic storm is the southward magnetic field in its flux rope, we speculate that if the CCs or HEs have stronger southward B_z as well. The cumulative fraction of maximum southward IMF larger than a certain value is shown in Figure 6. The ICMEs that are simultaneously CCs and MCs have the largest fraction compared to other subtypes related to the MCs, CCs, and the opposite types, shown in Figure 6(a). It becomes even more interesting when we consider the HE and its subtypes, shown in

Distribution of Single Storm Type on Storm Level (Samples Size:95 Single Storms)

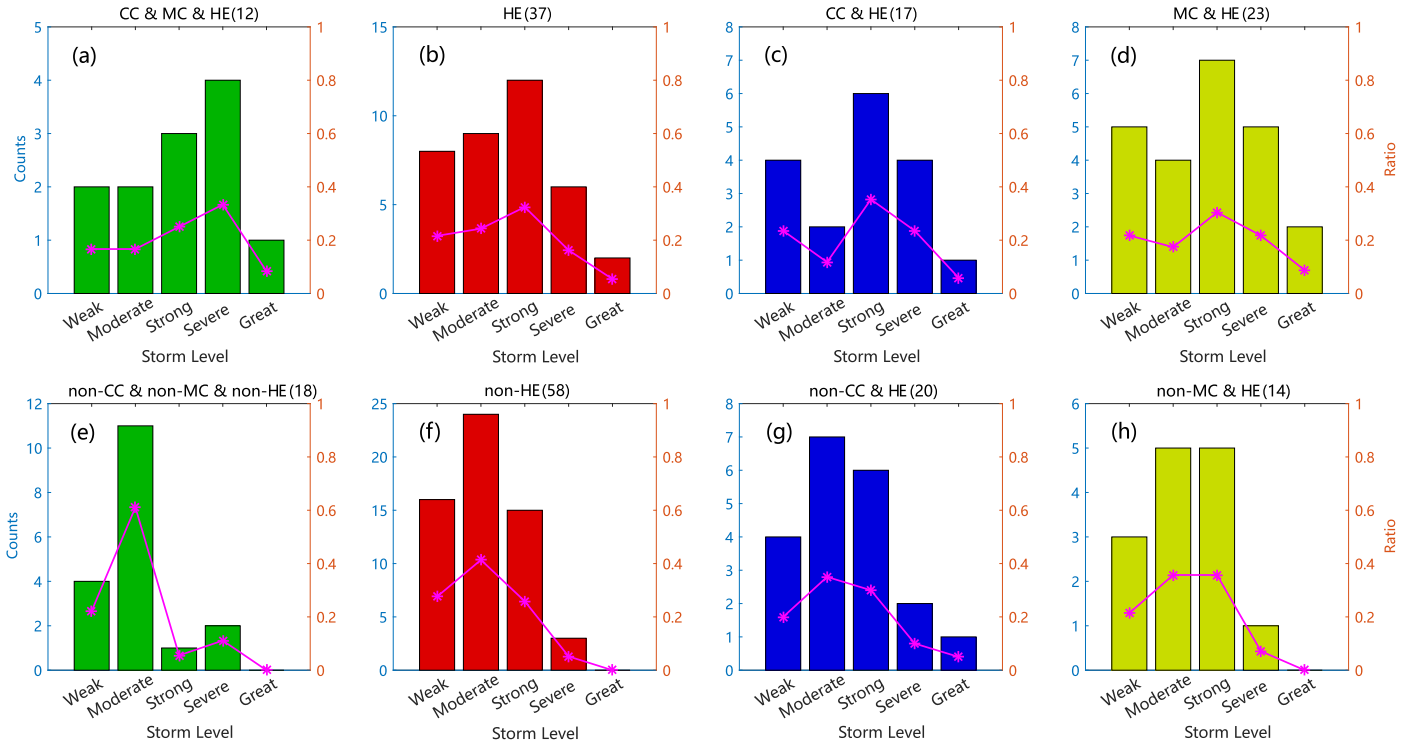


Figure 4. Distribution of 95 SSs caused by subtypes of ICMEs considering HEs. Panels (a)–(d) show the storm level distributions of SSs caused by CC&MC&HEs, HEs, CC&HEs, and MC&HEs, and panels (e)–(h) show those of SSs caused by the opposite types of ICMEs.

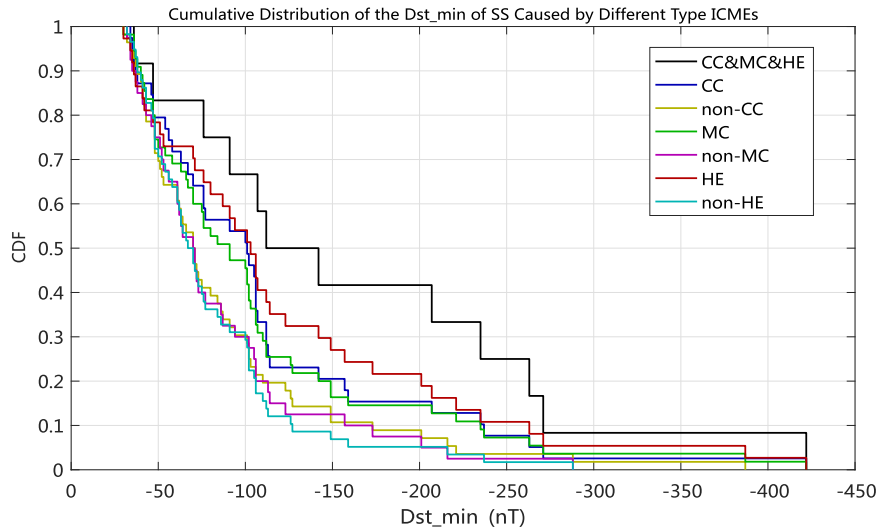


Figure 5. Cumulative distribution of Dst_{min} of the 95 SSs caused by different types of ICMEs. The x -axis is the Dst_{min} in units of nT. The y -axis is the cumulative distribution function (CDF).

Figure 6(b). The cumulative distribution of southward B_z of the 12 CC&MC&HEs have the highest value. It is well known that the solar prominence is featured by the low temperature and high helium abundance chromospheric material staying on the loops. According to Yan et al. (2015), the prominence in the active region (AR) could have twisted flux ropes formed by shear flow. The AR prominence could also stay with emerging flux ropes from the photosphere (Wang et al. 2019). Furthermore, jets are observed to transport a large amount of chromospheric material and magnetic field intensity from

lower atmosphere to AR prominence (Wang et al. 2018b). Therefore, the eruptive prominence is accompanied by enhanced twisted flux rope. This may explain why the ICMEs that are simultaneously the MCs, CCs, and HEs have the largest fraction containing strong southward magnetic field, which are most probable to generate magnetic storms, especially severe storms. Since the MCs are featured by the large-scale flux rope, and the CCs and HEs represent the cold prominence, respectively, in the CMEs. The ICMEs being CC&MC&HEs are related to the three-part CMEs in the solar

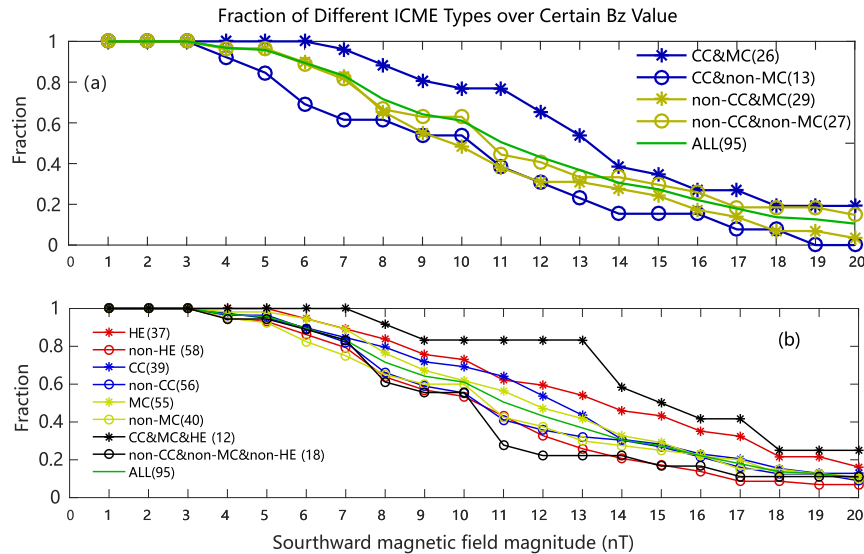


Figure 6. Fraction of ICMEs having southward IMF B_z larger than certain values. (a) The fraction of different subtypes related to the CCs and MCs having southward B_z larger than certain values. (b) The fraction of different types of 95 single ICMEs including the HEs.

corona. This means that the three-part CMEs have significantly stronger geoeffectiveness.

5. Conclusion

This work studies 219 ICMEs from 1998 to 2011, in which 95 single ICMEs causing 95 single magnetic storms. These ICMEs could be classified by carbon ionic charge signatures into 39 CCs and 56 non-CCs, or by magnetic flux rope structure into 55 MCs and 40 non-MCs, or by N_α/N_p into 37 HEs and 58 non-HEs. Out of the 95 ICMEs, 26 are simultaneously CCs and MCs, 17 are CC&HEs, and 12 are CC&MC&HEs. First, we examine the intensity level of all the 95 single storms and that of SSs caused by different subsets of ICMEs. The most probable intensity level of the 95 single storms is moderate. Differently, the intensity distribution of single storms caused by the CCs is concentrating at a strong level. The storms caused by the non-CCs have quite similar intensity distribution to the 95 SSs. It can be noted that more than half (6/11) of the severe and great storms are caused by the CC&MCs, and the CC&MC&HEs have the largest fraction (5/12) of severe and great storms of any other subset of ICMEs. It should be noted that the single storms caused by the CCs, MCs, and CC&MCs concentrate at a strong level, those caused by the CC&MC&HEs concentrate at severe level, and those caused by the non-CCs, non-MCs, non-HEs, and non-CC&non-MC&non-HEs mostly distribute at a moderate level. Besides, we use the KS-test to examine the difference in the cumulative distribution of Dst_{\min} of 95 SSs caused by different ICMEs. The result shows that the difference is significant at 95% confidence. The CC&MC&HEs have the highest cumulative fraction, followed by the HEs as the second highest, the CCs as the third, and the MCs as the fourth.

Next, we investigate the magnitude of southward IMF of the ICMEs. The CC&MC&HEs show a significantly larger fraction of $B_z < -11$ nT than any other subset of the ICMEs. Thus, whether or not the ICMEs are the MCs should not be the only variable to consider in evaluating their southward magnetic field and the magnetic storm level. The ion

composition should also be taken into account, as the erupted prominence is proved to have enhanced twisted flux ropes. We would like to conclude that the ICMEs related to the three-part CMEs containing both the large-scale flux rope and the cold prominence have the largest fraction of strong southward magnetic field and have the largest probability to cause strong and even higher level magnetic storms.

Our work suggests that both the prominence-inside ICMEs and MC ICMEs should be considered in evaluating the geoeffectiveness and in the space weather forecast. The ICMEs containing prominence material and large-scale flux ropes are related to the three-part CMEs on the solar corona. This means that the three-part CMEs are not only important for the study of the eruption mechanism in the source region, but also important for the study of space weather. Besides, another question that is raised from our work is why the different signatures of prominence material seldom occur in the same ICMEs simultaneously. Is it an effect of the spacecraft trajectory or a result of the prominence propagation in the heliosphere? The *Solar Orbiter* Mission to be launched in 2020 having the perihelion of 0.28 au will provide the best chance to locate and understand the same three-part CME from its origin to the heliosphere.

This work is supported by the Open Research Program of the Key Laboratory of Geospace Environment, Chinese Academy of Sciences (CAS), by the Fundamental Research Funds for the Central Universities, by National Natural Science Foundation of China (NSFC) under contract No. 41204125, and by the Chinese “111” project under contract No. B20011. The *ACE* and *WIND* data is from NASA CDA web. The ICME list is originally from the ACE Science Center. D. Li is thankful for the helpful discussion with Mr. Yaodong Xu.

Appendix

Table 2 presents single storm events and the related ICMEs from 1998 to 2011.

Table 2
95 Single Storms and the Related ICMEs Selected from Feng et al. (2018)

SN	ICME Start YYYY MM DD HHMM	MC Y/N	CC Y/N	HE Y/N	IMF B_z (nT)	Main Start YYYY MM DD HHMM	Dst _{min} Time YYYY MM DD HHMM	Recovery End YYYY MM DD HHMM	Dst _{min} (nT)
2	1998 Mar 4 1427	Y	Y	Y	-7.25	1998 Mar 4 1230	1998 Mar 4 1730	1998 Mar 5 1030	-36
9	1998 Jun 25 2131	Y	Y	N	-13.49	1998 Jun 25 1830	1998 Jun 26 0430	1998 Jun 26 1030	-101

(This table is available in its entirety in machine-readable form.)

ORCID iDs

Shuo Yao  <https://orcid.org/0000-0003-4267-0486>

References

- Adekoya, B. J., & Chukwuma, V. U. 2018, *AdSpR*, **61**, 274
 Akasofu, S.-I. 1981, *SSRv*, **28**, 121
 Burlaga, L., Sittler, E., Mariani, F., & Schwenn, R. 1981, *JGR*, **86**, 6673
 Burton, R. K., McPherron, R. L., & Russell, C. T. 1975, *JGR*, **80**, 4204
 Cane, H. V., & Richardson, I. G. 2003, *JGRA*, **108**, 1156
 Echer, E., Alves, M. V., & Gonzalez, W. D. 2005, *JASTP*, **67**, 839
 Feng, X., Yao, S., Li, D., Li, G., & Yan, X. 2018, *ApJ*, **868**, 124
 Forbes, T. G. 2000, *JGR*, **105**, 23153
 Forbes, T. G., Linker, J. A., Chen, J., et al. 2006, *SSRv*, **123**, 251
 Gonzalez, W. D., Joselyn, J. A., Kamide, Y., et al. 1994, *JGR*, **99**, 5771
 Gonzalez, W. D., Tsurutani, B. T., Gonzalez, A. L. C., et al. 1989, *JGR*, **94**, 8835
 Gopalswamy, N. 2006, *SSRv*, **124**, 145
 Gopalswamy, N., Yashiro, S., & Akiyama, S. 2007, *JGRA*, **112**, A06112
 Hirshberg, J., Bame, S. J., & Robbins, D. E. 1972, *SoPh*, **23**, 467
 Hudson, H. S., Bougeret, J.-L., & Burkepile, J. 2006, *SSRv*, **123**, 13
 Hundhausen, A. J., Sawyer, C. B., House, L., Illing, R. M. E., & Wagner, W. J. 1984, *JGR*, **89**, 2639
 Illing, R. M. E., & Hundhausen, A. J. 1985, *JGR*, **90**, 275
 Kilpua, E., Koskinen, H. E. J., & Pulkkinen, T. I. 2017a, *LRSP*, **14**, 5
 Kilpua, E. K. J., Balogh, A., von Steiger, R., & Liu, Y. D. 2017b, *SSRv*, **123**, 1271
 Lepri, S. T., & Zurbuchen, T. H. 2010, *ApJL*, **723**, L22
 Lin, J., & Forbes, T. G. 2000, *JGR*, **105**, 2375
 Loewe, C. A., & Prölss, G. W. 1997, *JGR*, **102**, 14209
 Maltsev, Y. P. 2004, *SSRv*, **110**, 227
 Manchester, W., Kilpua, E. K. J., Liu, Y. D., et al. 2017, *SSRv*, **212**, 1159
 Marsaglia, G., Tsang, W. W., & Wang, J. 2003, *J. Stat. Softw.*, **8**, 1
 Massey, F. J. 1951, *J. Am. Stat. Assoc.*, **46**, 68
 McCauley, P. I., Su, Y. N., Schanche, N., et al. 2015, *SoPh*, **290**, 1703
 McComas, D. J., Bame, S. J., Barker, P., et al. 1998, *SSRv*, **86**, 563
 Miller, L. H. 1956, *J. Am. Stat. Assoc.*, **51**, 111
 Monreal MacMahon, R., & Llop-Romero, C. 2014, *JASTP*, **114**, 66
 Nikolaeva, N. S., Yermolaev, Y. I., & Lodkina, I. G. 2011, *Ge&Ae*, **51**, 49
 Nikolaeva, N. S., Yermolaev, Y. I., & Lodkina, I. G. 2012, *Ge&Ae*, **52**, 28
 Ogilvie, K. W., Chornay, D. J., Fritzenreiter, R. J., et al. 1995, *SSRv*, **71**, 55
 Priest, E. R. (ed.) 1989, Dynamics and Structure of Quiescent Solar Prominences; Proc. Workshop (Dordrecht: Kluwer)
 Richardson, I. G., & Cane, H. V. 2004, *JGRA*, **109**, A09104
 Richardson, I. G., & Cane, H. V. 2010, *SoPh*, **264**, 189
 Schwenn, R., Rosenbauer, H., & Muehlhaeuser, K. H. 1980, *GeoRL*, **7**, 201
 Shewart, W. A., & Wilks, S. S. (ed.) 2004, The Comparison of Proportions from Several Independent Samples (New York: Wiley), 187
 Smith, C. W., L'Heureux, J., Ness, N. F., et al. 1998, *SSRv*, **86**, 613
 Song, H. Q., Zhang, J., Cheng, X., et al. 2019, *ApJ*, **883**, 43
 Song, H. Q., Zhong, Z., Chen, Y., et al. 2016, *ApJS*, **224**, 27
 Sugiura, M. 1964, *Ann. Int. Geophys. Year*, **35**, 9
 Wang, J., Feng, H., & Zhao, G. 2018a, *A&A*, **616**, A41
 Wang, J., Yan, X., Guo, Q., et al. 2019, *MNRAS*, **488**, 3794
 Wang, J., Yan, X., Qu, Z., et al. 2018b, *ApJ*, **863**, 180
 Webb, D. F., & Howard, T. A. 2012, *LRSP*, **9**, 3
 Wimmer-Schweingruber, R. F., Crooker, N. U., Balogh, A., et al. 2006, *SSRv*, **123**, 177
 Xie, H., Gopalswamy, N., Manoharan, P. K., et al. 2006, *JGRA*, **111**, A01103
 Yan, X. L., Xue, Z. K., Pan, G. M., et al. 2015, *ApJS*, **219**, 17
 Yao, S., Marsch, E., Tu, C.-Y., & Schwenn, R. 2010, *JGRA*, **115**, A05103
 Yashiro, S., Gopalswamy, N., Michalek, G., et al. 2004, *JGRA*, **109**, A07105
 Yermolaev, Y. I., Lodkina, I. G., Nikolaeva, N. S., & Yermolaev, M. Y. 2010, *CosRe*, **48**, 485
 Yokoyama, N., & Kamide, Y. 1997, *JGR*, **102**, 14215
 Zhang, J., Richardson, I. G., Webb, D. F., et al. 2007, *JGRA*, **112**, A10102
 Zurbuchen, T. H., & Richardson, I. G. 2006, *SSRv*, **123**, 31
 Zurbuchen, T. H., Weberg, M., von Steiger, R., et al. 2016, *ApJ*, **826**, 10